Controlled one-pot synthesis of PdAg nanoparticles and their application in the semi-hydrogenation of acetylene in ethylene rich mixtures

Jorge A. Delgado,*[a] Olivia Benkirane,[a] Suzanne de Lachaux,[a] Carmen Claver,[a,b] Joan Ferré,[c] Daniel Curulla-Ferré,[d] and Cyril Godard*[b]

[a] EURECAT, Centre Tecnològic de Catalunya, Carrer Marcel lí Domingo, 2-6, 43007 Tarragona (Spain).
[b] Universitat Rovira i Virgili, Departament de Química Física i Inorgánica, Marcel·lí Domingo, Campus Sescelades, 43007 Tarragona (Spain).
[c] Universitat Rovira i Virgili, Departament de Química Analítica i Química Orgànica, Marcel·lí Domingo, Campus Sescelades, 43007 Tarragona (Spain).
[d] Total Research and Technology Feluy, B-7181 Seneffe (Belgium)

Abstract

In the present paper, we report the synthesis of highly functionalized nanomaterials carefully nanoengineered to catalyze the semi-hydrogenation of acetylene in ethylene rich mixtures. Surface functionalization and structure modification of a series of bimetallic PdAg nanoparticles was performed using HHDMA as stabilizer and alloying the active palladium phase with silver. Bimetallic PdAg NPs with adjustable Pd/Ag ratio were prepared in water through a novel one-pot methodology using hydrogen gas as a benign reducing agent and cyanide as additive. UV-Vis studies indicated the formation of the bimetallic nanostructures through a sequential displacement-galvanic reduction process mediated by cyanide. The series of colloidal NPs were deposited onto alumina and successfully applied as catalysts in the selective hydrogenation of acetylene in ethylene rich mixtures. Geometric and electronic promotion of Ag over Pd based catalysts was evidenced by the increase of the ethylene selectivity with the Ag content. The reactivity of these materials demonstrated the applicability of HHDMA stabilized NPs in a gas phase reaction of industrial interest and the success of combining several strategies for the enhancement of the alkene selectivity.

Introduction

Over the last years, the industries of polymers and fine chemicals have experienced a revived interest for the development of highly selective catalysts for the semi-hydrogenation of alkynes. [1-4] Several transition metals were utilized for this transformation in which the main issues lay in the control of the over-hydrogenation, the polymerization of the alkynes or the isomerization of the alkene product.[5] Among the metals used, Pd has been identified as the most efficient in terms of activity although selectivity issues arise when utilized alone.[6] In spite of the availability of commercial options for the selective hydrogenation of alkynes such as the Lindlar or Pd Nanoselect catalysts, they frequently suffer limitations in terms of robustness[7] or accessibility constrains.[8] In addition, the recurrent necessity of including large amounts of nitrogen additives or toxic poisons such as Pb, have stimulated the development of more selective and environmentally friendly catalytic systems.[4, 9-11]

Current progress on nano-engineering offers a wide spectrum of possibilities for the preparation of highly functionalized nanomaterials with synergistic capabilities which could result in ultra-selective catalysts. When referred to the semi-hydrogenation of alkynes, most catalysts are transition metal based belonging to one of three categories: metal nanoparticles (M-NPs), metal nanoclusters (M-Clusters) and single-atom catalysts (SACs).[12, 13] For the specific case of the semi-hydrogenation of phenylacetylene and acetylene, single-atom catalysts based on Pd[13-17] or Cu[3] have demonstrated outstanding ethylene selectivity at high conversions, although these systems normally require relatively high temperatures (>100ºC) and the catalysts frequently involve very low metal loadings (<0.05wt%), which are both limitations for industrial applications. For the case of metal nanoparticles, two main types of functionalization for enhancing the selectivity can be distinguished: surface functionalization (e.g. stabilizing agent, core@shell, additives) and structural modifications (e.g. alloying, doping).[11]

Regarding surface functionalization of metal nanoparticles, surfactants are frequently used for their stabilization in aqueous media since they provide steric repulsion between particles.[18] For liquid phase reactions, a clear example that evidences the positive effect of the stabilizer on the performance of hydrogenation catalyst is the case of the Pd NanoSelect.[19, 20] This catalyst consists in palladium nanoparticles of 5-8 nm supported on carbon or titanium silicate that exhibit alkene selectivities comparable to those provided by the Lindlar's catalyst in the semi-hydrogenation of a broad range of alkynes and alkynols.[19] Pérez-Ramírez and co-workers investigated the selectivity patterns and accessibility constrains of Pd Nanoselect catalysts using experimental and theoretical approaches.[8] According to DFT calculations, the HHDMA stabilizer (hexadecyl(2-hydroxyethyl)dimethylammonium dihydrogen phosphate) is adsorbed rigidly over the Pd surface, which reduces both the number of active sites (geometric effect) and the hydride coverage at the Pd surface (electronic effect). These insights enlightened about the high alkene selectivity of the Pd Nanoselect catalysts.

In terms of structural modification, one of the main strategies of palladium based catalysts to enhance the alkene selectivity consists in the incorporation of a second metal,[21] in order to induce variations in the Pd electronic (e.g. charge transfer) and/or geometric properties (e.g. separation of Pd surface sites).[6] A wide variety of bimetallic combinations have been reported in the literature being palladium/silver one of the most relevant from the industrial point of view.[22] For instance, Mitsudome and co-workers reported the preparation of a series of core@shell Pd@Ag NPs with a diameter of *ca.* 26 nm with variable Ag content (9-33 wt% Ag) by deposition of a silver layer over Pd seeds by reduction of $AgNO_3$ using ascorbic acid in water.[23] In catalysis, excellent alkene selectivity was obtained in the semi-hydrogenation of 1-octyne under mild conditions using the Pd@Ag catalyst of 16.7 wt% Ag (>99% selectivity at >99% conversion at r.t and 1 bar H_2).

In spite of the remarkable high selectivity, the Pd loading required for these reactions was above 3 mol%, a value much higher than those usually required when Pd is used as the main active phase (e.g. 0.05-0.01 Pd mol% for PdCu or Pd NPs[24]). Although there are recurrent reports on PdAg NPs prepared by colloidal methodologies applied in the semi-hydrogenation of alkynes in liquid phase,[23, 25, 26] there is scarce information about the applicability of these type of NPs to gas phase reactions such as the semi-hydrogenation of acetylene in ethylene rich mixtures. The risk of site blocking by the stabilizer has hampered to a large extent the application of chemically stabilized NPs in gas phase reactions.[27, 28]

Here we report the synthesis of highly functionalized nanomaterials judiciously nanoengineered for catalytic purposes. A series of Pd and PdAg NPs with variable compositions (**50Pd50Ag**, **75Pd25Ag**, **90Pd10Ag** and **100Pd0Ag**) were prepared in water employing a novel methodology consisted in a one-step procedure employing Pd and Ag nitrate salts, HHDMA as stabilizer, hydrogen gas as a benign reducing agent and sodium cyanide as additive. The colloidal nanoparticles were supported onto α-alumina and evaluated in the selective hydrogenation of acetylene in ethylene rich mixtures demonstrating the applicability of HHDMA stabilized NPs in a gas phase reaction of industrial interest.

Results and discussion

Synthesis and characterization of colloidal bimetallic PdAg NPs

Bimetallic PdAg NPs were synthesized in water by simultaneous reduction of a mixture of $Pd(NO_3)_2$ and $AgNO_3$ in the presence of NaCN as additive, HHDMA as the stabilizer and using hydrogen gas as the reducing agent.

Complementary experiments analyzing the materials produced in presence or absence of NaCN or substituting the Ag precursor by $KAg(CN)_2$, suggested the central role of cyanide for the effective formation of bimetallic nanostructures (Supporting Information, Figure S1-S7). The effect of the CN:Pd ratio was studied in the range between 0.66-3:1. It was observed that PdAg NPs are only formed for CN:Pd ratios between 2-2.5:1. Ratios lower than 2 resulted in the formation of mixtures of monometallic Pd and Ag NPs, while higher than 2.5 resulted in the formation of irreducible Pd species (e.g. $Pd(CN)_{2(s)}$) and only Ag NPs were obtained.

Several reaction parameters were evaluated using design of experiments (DOE) with the aim to study their impact on the particle size and dispersity of **50Pd50Ag** bimetallic NPs (Supporting Information, section 2.3). The reaction parameters selected for optimization were: temperature, metal concentration, CN:Pd ratio and hydrogen pressure. Based on the obtained results of the initial matrix of experiments followed by a simple refining, NPs in the range of 9.9 – 8.3 nm were obtained. The conditions providing the smallest particle size and lowest dispersity (8.31 ± 2.65 nm) were the following: 110 ºC, CN:Pd ratio = 2:1, 7 mM of metals, 5 bar, HHDMA = 10, 2h. Subsequently, the conditions used for the synthesis of **50Pd50Ag** were extended for the preparation of NPs of molar compositions, **75Pd25Ag** and **90Pd10Ag**. A reference of monometallic nanoparticles (**100Pd0Ag**) were also prepared using an analogous methodology. In all cases, homogenous colloidal suspensions were obtained. Interestingly, the increase in Pd content of the bimetallic NPs from 50 to 90 mol% resulted in the progressive decrease of the particle size from 7.3 nm to 3.8 nm respectively (Figure 1).

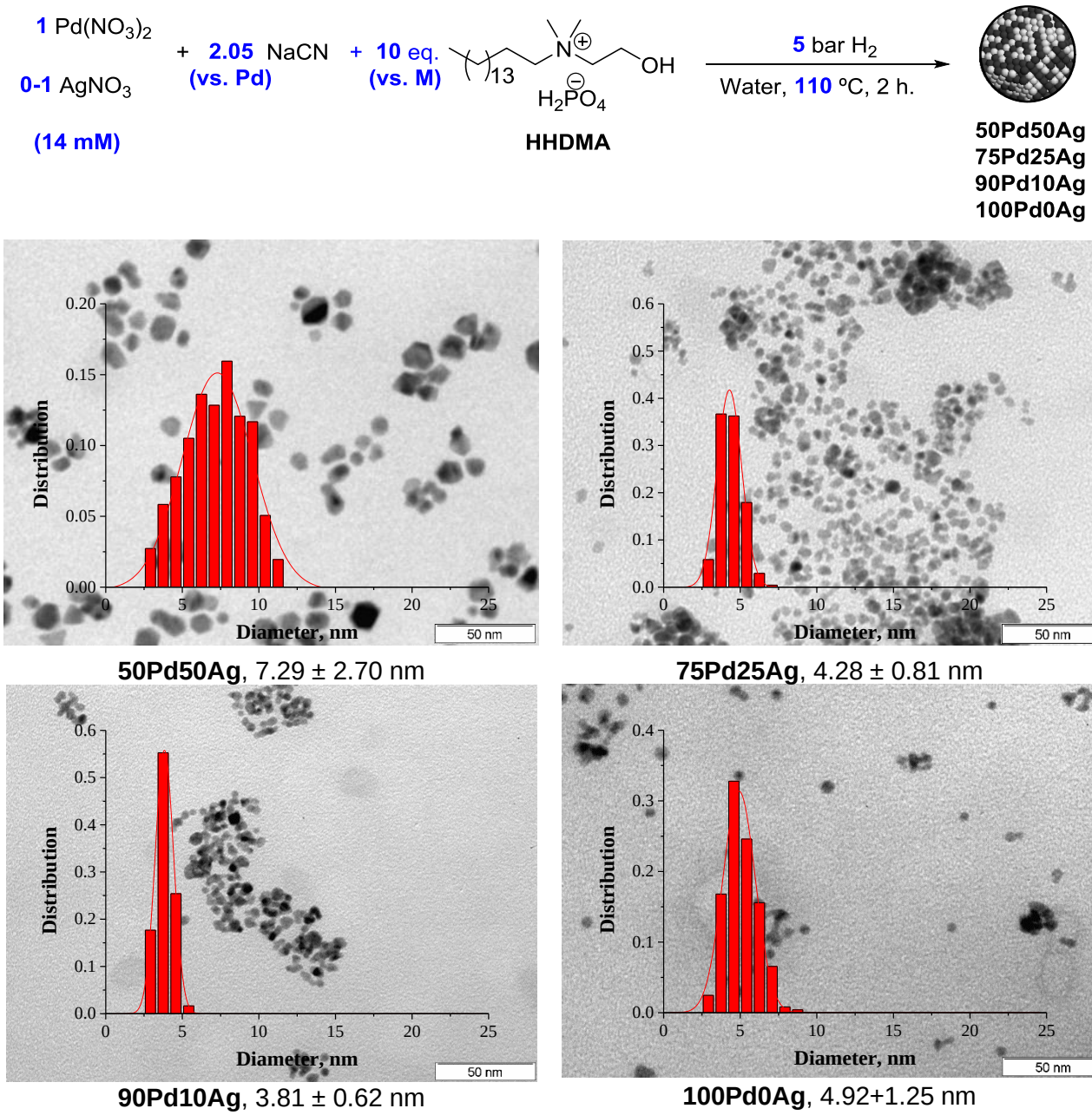

Figure 1. TEM micrographs and size histograms of PdAg NPs of variable composition and monometallic Pd NPs.

The obtained colloidal nanoparticles were isolated and characterized using various techniques. Analysis by XRD revealed the formation of bimetallic alloyed structures with the detection of diffraction peaks at intermediate positions between the pure Pd and Ag references (Figure 2). The position of the peaks is progressively displaced as a function of the metal composition. The lattice constant obtained for these NPs evidenced a linear relationship with the Pd content, (Figure 2b) in agreement with fully alloyed PdAg structures. Interestingly, the lattice parameters of these nanostructures evidenced a positive deviation from ideal Pd or PdAg mixtures (Supporting Information, Figure S17). Lattice expansion could be explained by the presence of interstitial carbon in the metallic structure of the nanoparticles occurring during the aqueous synthesis (C-doping), as documented by other authors.[29, 30] The crystallite sizes estimated by XRD confirmed

the TEM observations, with the decreasing size of the NPs as the Pd content increased (3.2, 2.6 and 2.4 nm for **50Pd50Ag** a **75Pd25Ag** and **90Pd10Ag** respectively).

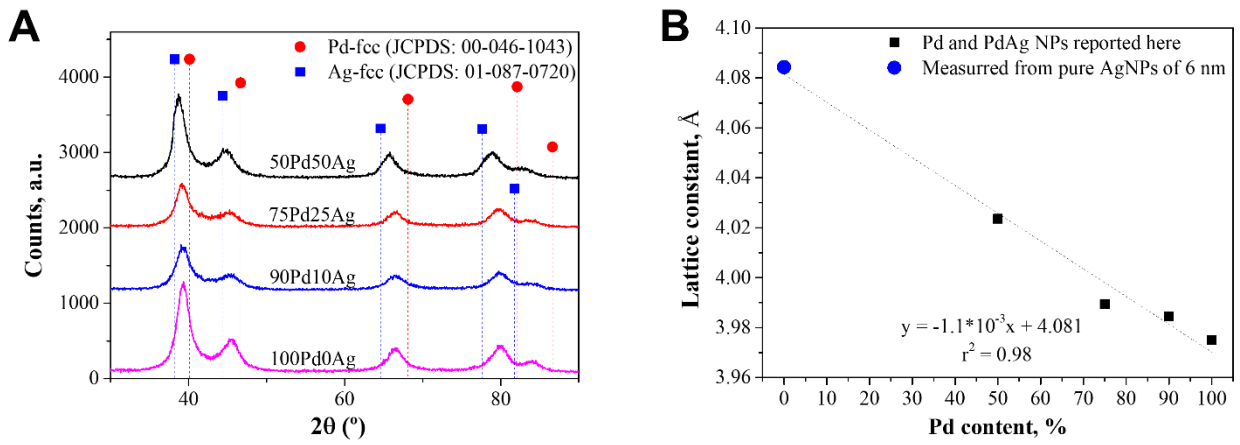

Figure 2. (A) XRD diffractogram and (B) relationship between the lattice constant and the Pd content for the series of NPs.

Analysis by UV-Vis of **50Pd50Ag** revealed the presence of a plasmon band of Ag centered at 350 nm, a wavelength characteristic of PdAg alloys.[31] For the case of **75Pd25Ag** and **90Pd10Ag,** alloying of the metal surface is suggested by the presence of a shoulder in the region of 300-400 nm which decreased progressively in intensity when the silver content decreases (Supporting Information, Figures S18 and S19). Such a shoulder disappears completely for the case of **100Pd0Ag** in which silver is not present. It was thus concluded that the series of PdAg exhibits a bimetallic alloyed surface, in agreement with their nominal composition.

To gain further insights regarding the bulk and surface composition of the series of NPs, the Pd and Ag content was studied by ICP and XPS (Supporting Information, Table S6). The mol% of Pd and Ag determined by both techniques were in close agreement with the nominal values, thus confirming the homogenous distribution of the metals in both, the bulk and the surface of the NPs.

To examine the metal speciation at the surface of the PdAg NPs, XPS analysis of the Pd 3d and Ag 3d orbitals were carried out. In these analyses, charging effects were automatically compensated using a charge neutralizer. The Pd and Ag peak intensities for the series of NPs were consistent with the corresponding metallic compositions (Figure 3), an observation documented previously by other authors.[32]

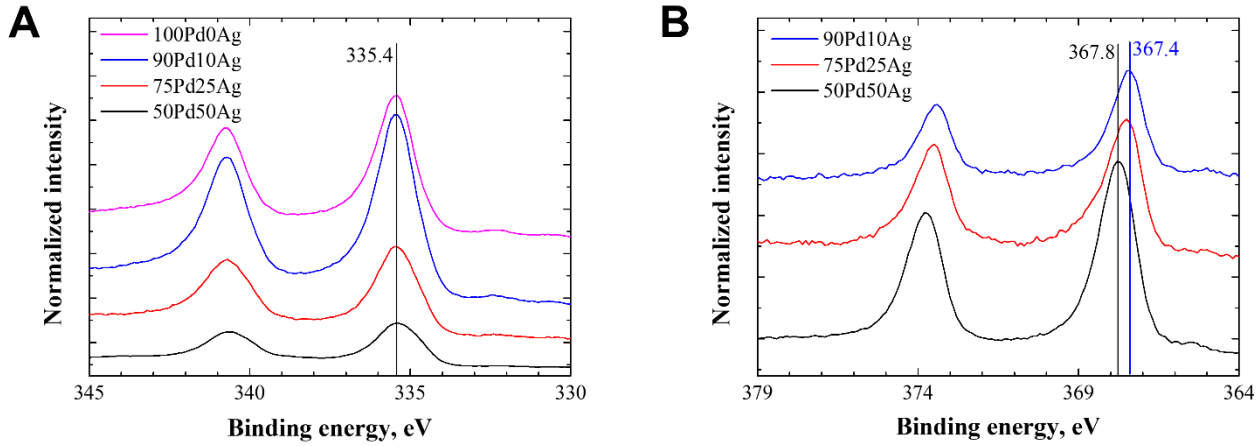

Figure 3. (A) Pd 3d and (B) Ag 3d XPS spectra of monometallic and bimetallic PdAg NPs

The Pd 3d peaks of the whole series of bimetallic and monometallic NPs were centered at practically the same binding energies (BE shifts <0.2 eV), at 335.4 and 340.7 eV. Observations of small shifts in Pd 3d peaks were also reported by Monnier and co-workers for the case of supported PdAg/SiO_2 catalysts prepared by electroless deposition and by Deganello and co-workers for pumice-supported Ag–Pd catalysts.[33-35]

In order to study the effect of alloying on the oxidation state of silver in the bimetallic catalysts, the binding energy of Ag $3d_{5/2}$ peaks were measured and compared with the value reported for the monometallic reference (BE Ag^0, 368.2 eV).[36] The binding energy shifts ($BE_{ref} - BE_{sample}$) were therefore plotted against the silver content (Supporting Information, Figure S22). For all bimetallic compositions, the BE of Ag $3d_{5/2}$ peaks were lower than the corresponding reference in about 0.4-0.8 eV. Similar observations of negative shifts of the Ag binding energy for PdAg alloyed catalysts were also documented by Deganello and co-workers, a phenomena attributed to electronic interactions between silver and palladium atoms.[34, 35, 37] Consequently, the relatively large negative shift of the Ag BE observed on **90Pd10Ag** (0.8 eV) is a result of the degree of the interaction of the valence orbitals between Ag and Pd, maximized under situations of large dilution of Ag over the Pd phase.[37]

Insights into the mechanism of formation of bimetallic 50Pd50Ag NPs

In order to gain insights into the mechanism of formation of bimetallic PdAg NPs, the evolution of the plasmonic response in the UV-Vis of the NPs was monitored over time. For this purpose, the synthesis of **50Pd50Ag** NPs was performed under standard conditions, and samples of the colloidal suspension were extracted at different times under constant hydrogen pressure and analyzed by UV-Vis spectroscopy and TEM. The collected spectra and a detailed description of the observed correlations are included in the Supporting Information (Section 2.4).

Insights into the formation mechanism of the PdAg NPs were obtained by analyzing the evolution of plasmon band maximum and its intensity, an approach analogous to the one reported by Iglesia et al. for the case of AuPd NPs.[38] For instance, at initial reaction times (t = 1.3 min) a plasmon band maximum at 379 nm is in agreement with a bimetallic PdAg structure at the surface.[31] The unsymmetric nature of this band also support this observation. Subsequently, between 2.3 and 4.8 min, the plasmon band shifted to *ca.* 392 nm exhibiting a more symmetric Gaussian shape, in agreement with NPs with a silver rich surface. In the interval from 4.8 to 6.0 min, the plasmon band maximum exhibited a dramatic decrease, from 393 to 363 nm, suggesting the alloying of the surface. From 6.0 min till 90-120 min, such a maximum decreased progressively from 363 till 346 nm suggesting the enrichment of the NPs surface by Pd or the decrease in particle size. These changes in the surface composition of the PdAg NPs can result from segregation of Pd towards the NPs surface promoted by either molecular hydrogen, or cyanide in combination with the reaction temperature employed.

Based on the experimental evidence, a mechanism of formation of PdAg NPs is proposed, which is comprised by three main stages (Figure 4, I-II-II). At early reaction times, bimetallic clusters are formed with a marked PdAg alloyed nature at the surface (I-a). Next, the bimetallic clusters grow, resulting at the beginning in NPs with a silver rich surface (I-b) and subsequently in NPs with an alloyed surface (I-c). Once the metallic precursors are consumed through a Ag/Pd galvanic substitution-redeposition process (II), the NPs start a restructuration process in which the Ag ensembles at the surface are progressively diluted probably because

of segregation of Pd from the core towards the NPs surface (III). Combining the UV-Vis spectroscopic analysis with information of the evolution of the TEM particle size over time, it was concluded that the formation of bimetallic PdAg NPs occurs by a sequential displacement–reduction process. With a similar approach to the one presented here, Iglesia et al. also provided mechanistic evidence for sequential displacement–reduction routes during the synthesis of PdAu clusters.[38]

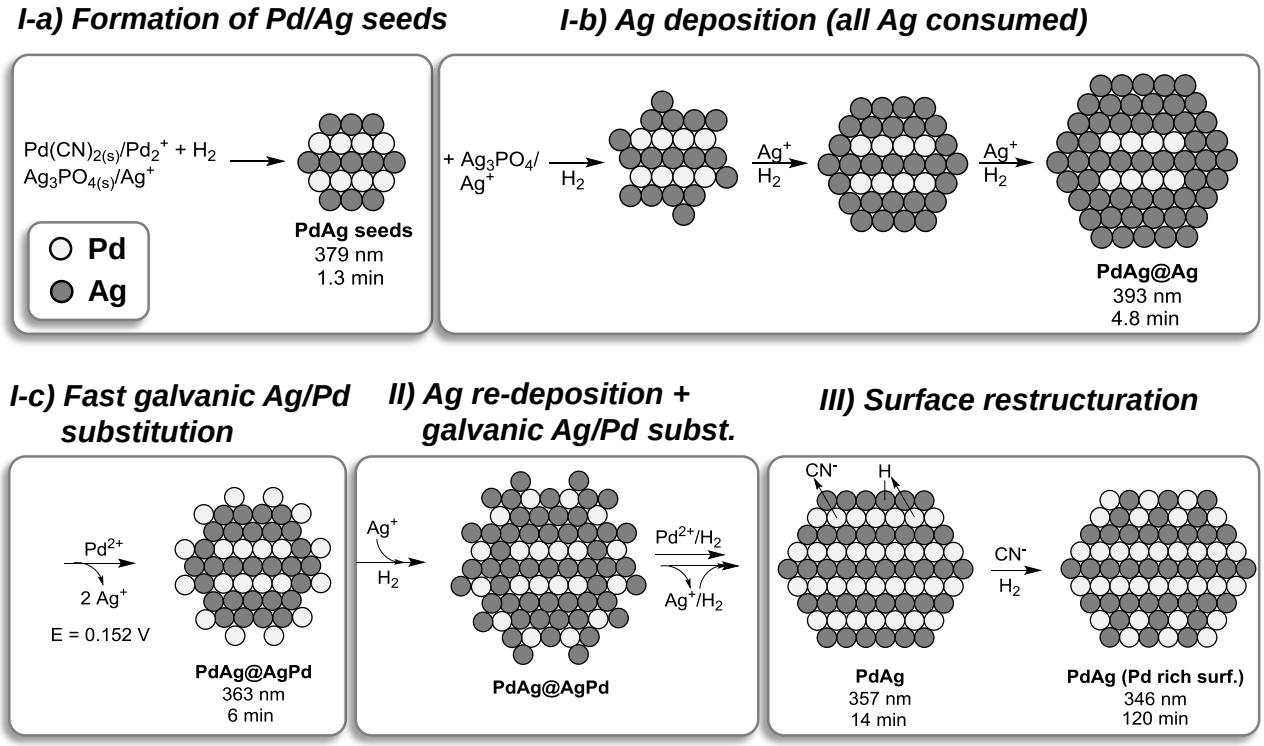

Figure 4. Proposed mechanism of formation of bimetallic PdAg NPs

Synthesis and characterization of* α-Al_2O_3 *supported PdAg/*Al_2O_3 *catalysts

TEM analysis of the alumina supported catalysts evidenced a good dispersion of the NPs onto the support (Supporting Information, Figure S23). The particle sizes measured for the supported catalysts were in agreement with those observed for the corresponding colloidal NPs.

The fine structure of **50Pd50Ag/Al_2O_3** catalyst can be appreciated in the HR-TEM micrograph displayed in Figure 5a. A profile analysis of the bimetallic nanoparticles revealed a d-spacing of 2.317 Å corresponding to the plane 111 of a face centered cubic (fcc) structure, value that matches that obtained from the electron diffraction (inset). The measured d-spacing has an average value compared to the reported for the same plane in pure Pd and Ag fcc structures (2.285 and 2.354 Å respectively),[39, 40] in agreement with a fully alloyed structure. A similar analysis performed on **75Pd25Ag/Al_2O_3** (Supporting Information, Figure S25) revealed a d-spacing of 2.302 Å for the same plane, a value that agrees with the increase of the Pd content. Figure 5b displays the fine structure of a nanoparticle of **75Pd25Ag/Al_2O_3** acquired by STEM-HAADF. Reconstruction of this particle based on the contrast exhibited by the different faces suggested a cubo-octahedron shape typical

of fcc metallic nanostructures. Additional micrographs for the series of bimetallic and monometallic catalysts are displayed in the Supporting Information (Figures S24-S27).

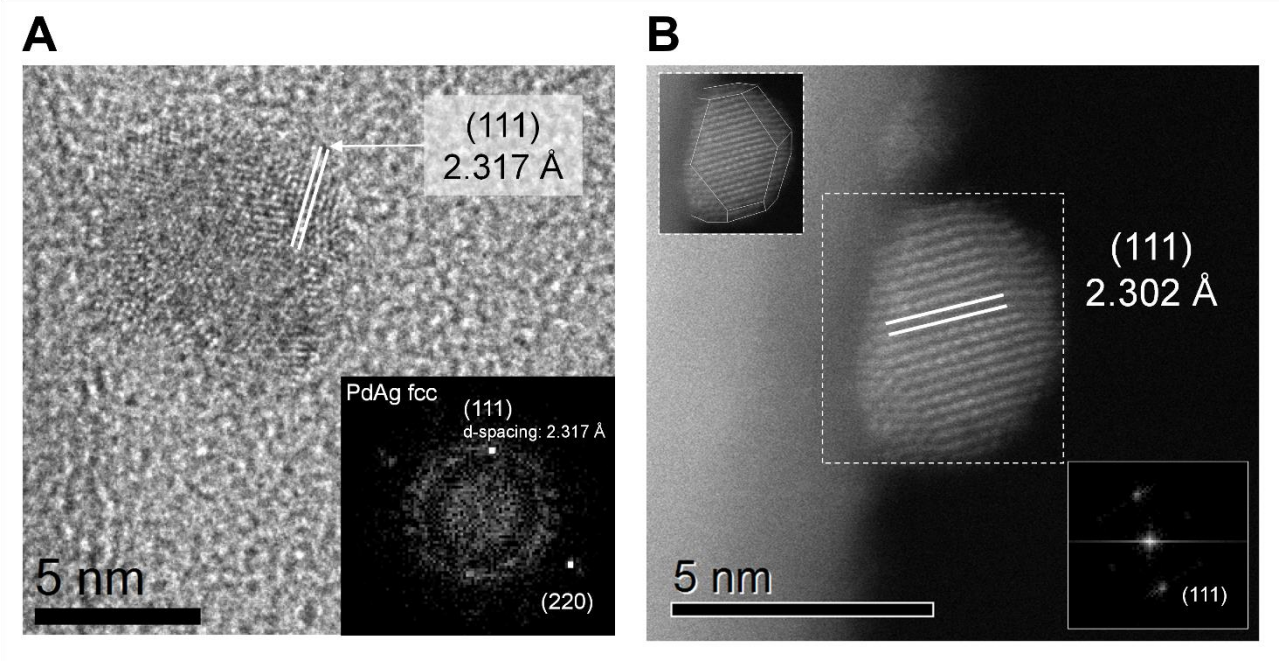

Figure 5. (A) High resolution micrograph and electron diffraction (FFT) of a nanoparticle in **50Pd50Ag/Al_2O_3** catalyst. (B) STEM-HAADF micrograph, electron diffraction (FFT) and reconstruction of a nanoparticle in **75Pd25Ag/Al_2O_3** catalyst.

The metallic composition of individual nanoparticles was studied by STEM-HAADF/EDS analysis. Analysis of at least 10 NPs were carried out and averaged for statistical purposes. The obtained molar compositions for the series of bimetallic nanoparticles were 52Pd48Ag, 72Pd28Ag, 91Pd10Ag, values which are in close agreement to the nominal ones (**50Pd50Ag**, **75Pd25Ag**, **90Pd10Ag**). This observation confirms the bimetallic nature and the composition of the prepared nanoparticles at the nano-scale. To gain further insights about the metal distribution, elemental mappings of Pd and Ag were performed on individual nanoparticles.

Figure 6 displays the STEM-HAADF analysis of nanoparticles of the three bimetallic catalysts with the corresponding EDS elemental maps for Pd and Ag. In the three cases the Pd and Ag distribution was homogeneous along the nanoparticles, characteristic also confirmed by EDS elemental analysis in line (Supporting Information, Figure S27). These observations are consistent with the formation of fully alloyed PdAg structures.

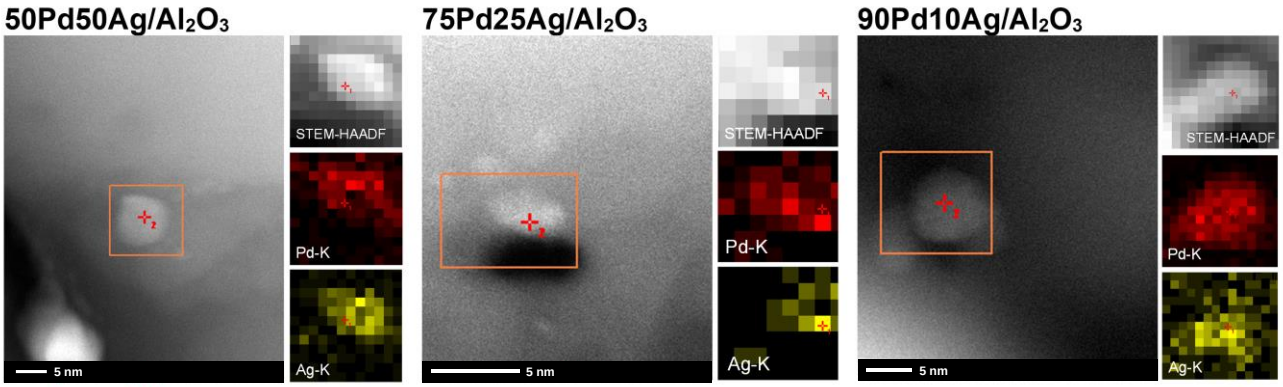

Figure 6. STEM-HAADF micrographs of single metal NPs of supported bimetallic catalysts with the corresponding EDS elemental maps for Pd and Ag.

Analysis of the supported catalysts by FTIR and TGA indicated the presence of the HHDMA stabilizer in trace amounts (Supporting Information, Figures S31-S32). ICP analysis of digested samples of supported catalysts indicated that in all the cases, the Pd and Ag metal loadings were in close agreement to the nominal values (nominal Pd loading, 0.4-0.5 wt%, Supporting Information, Table S8).

Summarizing, extensive characterization on colloidal and supported PdAg bimetallic catalysts afford solid evidence about the fully alloyed structure at the surface and bulk of the nanoparticles. For the series of catalysts with variable Pd/Ag formulation, the composition and metal distribution at the micro and nanoscale finely match the nominal values.

Semi-hydrogenation of acetylene in excess ethylene

The series of supported catalysts was tested in the selective hydrogenation of acetylene in excess ethylene. The employed reaction feed stream roughly approximate the tail-end feed of an ethylene cracker: 1% C_2H_2, 20% C_2H_4, 5% H_2, balance N_2.[32, 41] The reactions were carried out in a micro fixed-bed reactor at 50 ºC and 1 bar. The catalytic tests were performed at iso-conversion mode at a fixed value of 70%. Reaction parameters such as the reaction rate and selectivity were monitored during the first 24-48h.[42] As a general observation, the reaction rate of a fresh catalyst generally started in a relatively high value, and then decreased smoothly over time. Such a decrease in activity is typically ascribed to catalyst deactivation probably because of carbon deposits.[42]

For comparison purposes, two commercial palladium catalysts were also tested under identical reaction conditions. The first reference was the Pd Nanoselect catalyst (ref. LF200), which consisted in PdNPs of 7 nm stabilized by HHDMA and supported on titanium silicate. The second reference consisted in a supported monometallic Pd/Al_2O_3 catalyst (Strem Chemicals) comprised by PdNPs of 3 nm. Table 1 describes relevant physical properties of the tested catalysts.

Table 1. Physical properties of catalysts evaluated in the selective hydrogenation of acetylene in excess ethylene.

Nº	Catalyst	Pd, wt%	Ag wt%	M-mol% Pd	TEM particle size, nm	Fraction of Pd surface atoms*
1	**100Pd0Ag/Al_2O_3**	0.406	0.000	100	4.92	0.264
2	**90Pd10Ag/Al_2O_3**	0.452	0.038	92	3.81	0.305
3	**75Pd25Ag/Al_2O_3**	0.425	0.138	76	4.28	0.226
4	**50Pd50Ag/Al_2O_3**	0.366	0.303	55	7.29	0.101
5	**Pd Nanoselect LF200**	0.398	0.000	100	7.00	0.190
6	**Pd/Al_2O_3-3nm**	0.480	0.000	100	3.00	0.404

* The fraction of Pd surface atoms was calculated based on Van Hardeveld-Hartog statistics of ideal fcc metallic nanostructures,[43] and the Pd molar fraction determined in the catalyst by ICP. Considering the similitude of the atomic radii of Pd and Ag, the calculation of the fraction of surface Pd atoms was made using only the radii of Pd.

The evolution of the activity and TOF as a function of the time is displayed in Figure 7. In terms of activity, catalysts **100Pd0Ag/Al_2O_3**, **90Pd10Ag/Al_2O_3** and **75Pd25Ag/Al_2O_3** displayed stable activities of *ca.* 1500 mol C_2H_2 mol_{Pd}^{-1} h^{-1} in the range between 4-12h (period corresponding to the steady state, Figure 7a). After 12h, all of them exhibited a progressive decrease of the rate, associated to deactivation processes. The deactivation rates followed the order **50Pd50Ag/Al_2O_3** < **75Pd25Ag/Al_2O_3** < **90Pd10Ag/Al_2O_3** < **100Pd0Ag/Al_2O_3** being inversely proportional to the amount of silver.

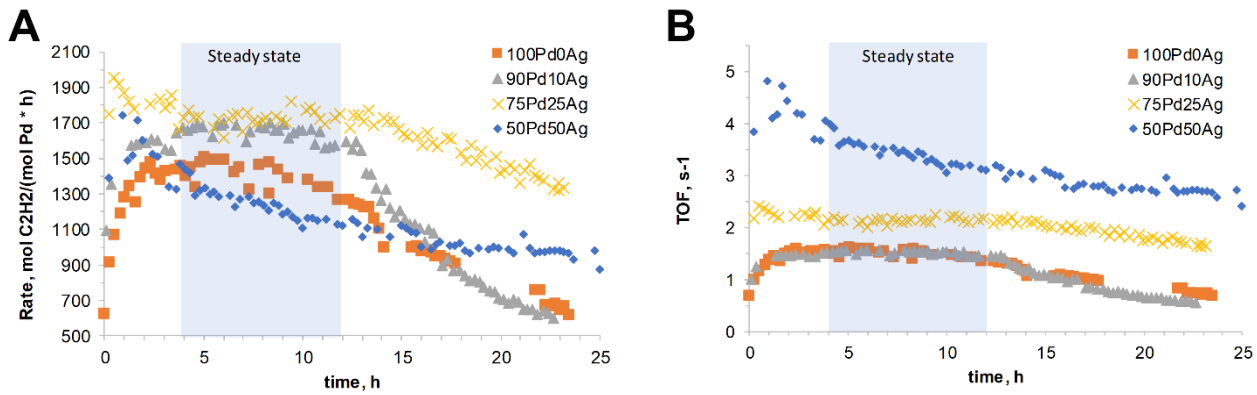

Figure 7. Evolution of the reaction rate (A) and TOF (B) during the time obtained for the series of $PdAg/Al_2O_3$ catalysts. Conditions: 0.1 mg Pd, 50 ºC, 1 bar, variable total flow (140-40 ml/min, for iso-conversion of acetylene at 70%).

Since the Pd surface sites are meant to decrease with the Ag content (according to a fully alloyed structure), a fair comparison of these catalysts requires the determination of specific activities per exposed Pd sites (turn over frequency, TOF). Figure 7b displays the TOF values for C_2H_2 conversion and C_2H_6 formation for the series of catalysts. Details about the calculation basis of TOF values (and the estimation of the fraction of Pd surface atoms) are included in the Supporting Information (Section 4.1). As displayed in Figure 7b, the TOF values increased with the Ag content: at 12 h of reaction TOF values were, 1.3, 1.4, 2.0 and 3.1 s^{-1} for **100Pd0Ag/Al_2O_3, 90Pd10Ag/Al_2O_3, 75Pd25Ag/Al_2O_3** and **50Pd50Ag/Al_2O_3** catalysts, respectively. Based on reports from other authors, the higher TOFs observed for catalysts with high Ag content might be a consequence of the dominant acetylene adsorption as π-bonded species which require less Pd sites, and are possibly hydrogenated faster in comparison with other adsorption modes (e.g. multi-σ-bonded species) prevalent at lower Ag contents.[41, 44,45]

The evolution of the selectivity during the time is displayed in Figure 8. In all the cases, the ethylene selectivity (C_2H_4, depicted in blue) decreased smoothly over time at a rate function of the Ag content: the higher the Ag content the slower such a decrease, being minimized for the case of **50Pd50Ag/Al_2O_3**. The C_2H_6 selectivities showed the opposite trend. It is noteworthy that the ethylene selectivity of **50Pd50Ag/Al_2O_3** was markedly more stable than those of the other catalysts of the series, with selectivity values for C_2H_4 up to 75-85%. Even after extended reaction times (50 h), this catalyst exhibited a very low deactivation rate. For this case, the C_{4s} selectivity remained almost unchanged during 50 h of reaction, differently to other catalysts with less silver content, which exhibited decreases of C_{4s} percentage of *ca.* 4% in 24 h reaction runs (generally from 8 to 4 %).

Based on these results, **50Pd50Ag/Al_2O_3** clearly displayed superior catalytic performance as a consequence of the largest content of silver which could exert both geometric and electronic positive impact in catalysis. The observed profile of selectivities is consistent with the assumptions proposed earlier for the rationalization of TOF values in terms of geometric promotion of Pd by Ag. For instance, Monnier and co-workers proposed that in PdAg formulations of high Ag contents (which result in small ensembles of Pd sites), acetylene is adsorbed as a π-bonded species that favors hydrogenation to ethylene. In contrast, at low Ag contents, where ensemble sizes of Pd sites are larger, acetylene is strongly adsorbed as a multi-σ-bonded species which preferentially forms ethane, lowering the ethylene selectivity.[41] The effect of Ag content on the selectivity can also be correlated with available DFT data in terms of adsorption energies for representative carbon species adsorbed on equivalent alloyed surfaces (Supporting Information, Figure S35).[46] The trends in adsorption energy of CH* and CH_2* (as analogous of acetylene and ethylene respectively) suggest a weaker adsorption of both adsorbates with the increase of silver content, which might explain the selectivity increase due to the favored desorption of the ethylene product from the metal surface. The selectivity values displayed by the presented bimetallic catalysts, are comparable with PdAg/Al_2O_3 catalysts of variable composition reported by Pachulski et al.[42] and Zhang et al. [32, 41] Detailed comparison between the catalytic data described here and those previously reported is included in the Supporting Information (Section 4.3).

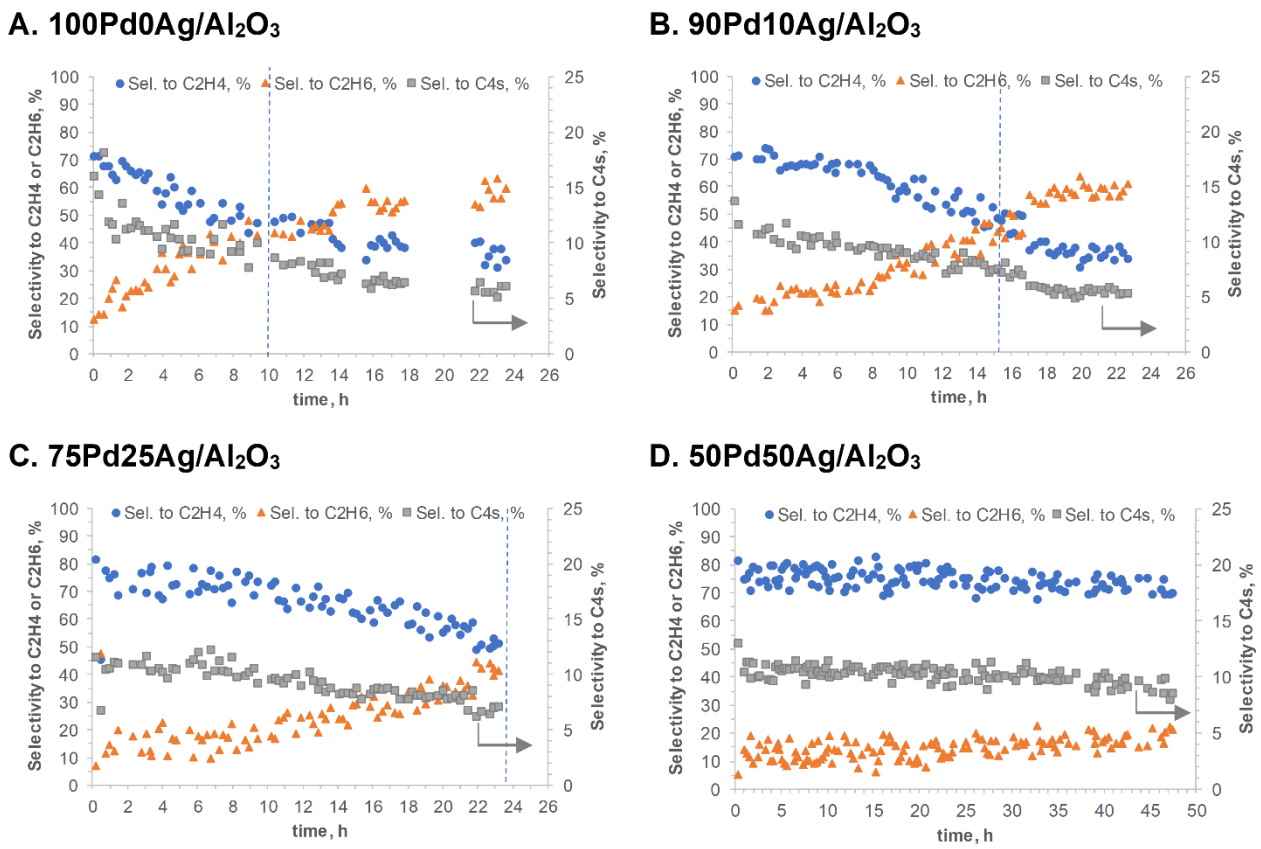

Figure 8. Evolution of the selectivity (towards C_2H_4, C_2H_6 and C_4s) during the time obtained for the series of $PdAg/Al_2O_3$ catalysts. Conditions: 0.1 mg Pd, 50 ºC, 1 bar, variable total flow (140-40 ml/min, for iso-conversion of acetylene at 70%).

Considering that **50Pd50Ag/Al_2O_3** catalyst displayed the best catalytic performance of the tested series, the preparation of a catalysts provided with higher Ag content was attempted by extending the synthesis methodology for the colloidal NPs (25Pd75Ag). Unfortunately, segregation of Ag and Pd NPs was observed in the obtained colloid. Limitations of the current recipe might be associated to the strict equilibria between the Pd-Ag species in relation with the equivalents of cyanide present in solution (Supporting Information, Scheme S1)."

Next, the monometallic reference catalysts were evaluated in the semi-hydrogenation of acetylene under the same reaction conditions (**Pd Nanoselect LF200** and **Pd/Al_2O_3-3nm,** Supporting Information, Figure S34). A prominent decrease of the reaction rate was registered from the beginning of the reaction in both cases, evidencing an extended catalyst deactivation. After 5h the rate in **Pd/Al_2O_3-3nm** seemed to be stabilized at a relatively low value, 0.3 s^{-1}, thus suggesting that most of the deactivation occurred during this period. According to Claus and co-workers, in pure palladium catalysts, the number of dissociatively adsorbed acetylene molecules is relatively higher in comparison to bimetallic PdAg surfaces, resulting in the formation of green oil, coke and ethane.[42] Due to these side reactions, higher deactivation rates and lower TOF values occur on monometallic Pd catalysts, when compared to bimetallic PdAg ones.

In terms of selectivity, **Pd Nanoselect LF200** started the reaction with a relatively high C_2H_4 selectivity (*ca.* 80%) but quickly decreased to 50% during the first 8h of reaction, thus indicating a fast deactivation profile (Figure 9). **Pd/Al_2O_3-3nm** exhibited poor ethylene selectivities during the whole run (*ca*. 40%), although this

value was stable during the time. Interestingly, the selectivity profile exhibited by the **Pd Nanoselect LF200** was very similar to the one of **100Pd0Ag/Al_2O_3**, both being markedly different to the one displayed by **Pd/Al_2O_3-3nm**. This observation suggests that the presence of HHDMA (in **Pd Nanoselect LF200** and **100Pd0Ag/Al_2O_3**) might contribute to the high ethylene selectivity at early reaction stages. It is also noteworthy that the deactivation rate of **100Pd0Ag/Al_2O_3** was lower than the one of **Pd Nanoselect LF200** (TOFs of 1.5 vs. 0.5 s^{-1} at 6h respectively). Considering that the two catalysts are both based on Pd and stabilized by HHDMA, other structural differences such as the C-doping occurring in **100Pd0Ag/Al_2O_3** (as evidenced by XRD analysis) might be the responsible of the enhanced stability for this catalyst. Other authors have also accounted on the positive impact on the catalytic performance after doping the Pd active phase with interstitial atoms such as C or B. For instance, Tsang and co-workers evaluated the use of palladium nanoparticles with interstitial carbon atoms as a catalyst for the hydrogenation of 3-hexyn-1-ol and 4-octyne.[47] It was found that the Pd nanocatalyst with subsurface carbon substantially reduced undesirable over-hydrogenation and isomerization reactions. This observation was justified by the increase in the desorption rate of the alkene species as a result of the hybridization of the Pd d-state with the C sp-state.

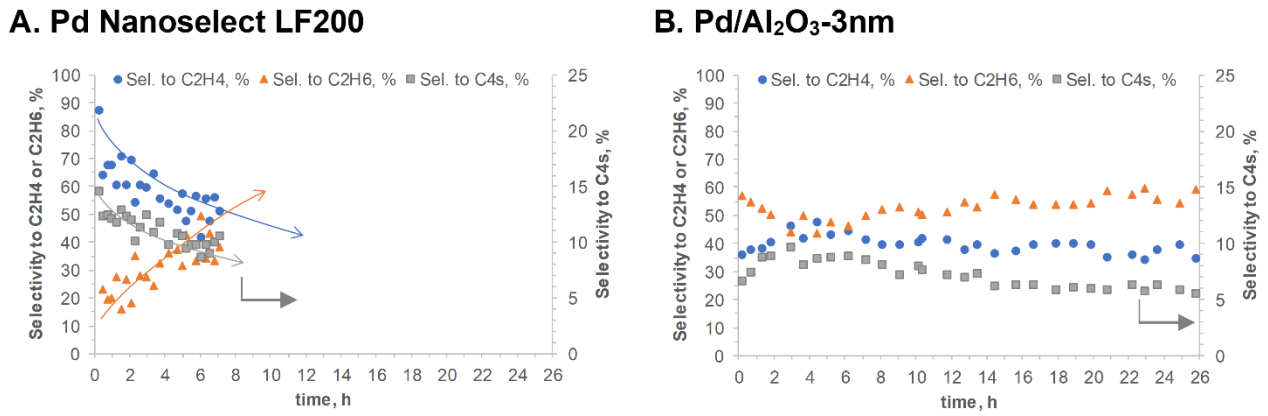

Figure 9. Evolution of the selectivity (towards C_2H_4, C_2H_6 and C_4s) during the time obtained for reference catalysts: (A) Pd **Nanoselect LF200** and (B) **Pd/Al_2O_3-3nm**. Conditions: 0.1 mg Pd, 50 ºC, 1 bar, variable total flow (140-40 ml/min, for iso-conversion of acetylene at 70%).

Summarizing, a series of bimetallic PdAg/Al_2O_3 with variable PdAg composition were evaluated in the selective hydrogenation of acetylene in ethylene rich mixtures. From the tested catalysts, **50Pd50Ag/Al_2O_3** displayed the highest and most stable TOF values along the run, and the deactivation rate was markedly lower compared the other catalysts with lower silver contents. The ethylene selectivity for this case was also superior and stable at extended reaction times (ca. 80% after 48h of reaction).

Conclusions

A series of mono and bimetallic NPs with variable composition, **50Pd50Ag, 75Pd25Ag, 90Pd10Ag** and **100Pd0Ag** were prepared in water employing a novel methodology. The synthesis consisted in a one-step approach employing the nitrate salts of both metals, HHDMA as stabilizer, hydrogen gas as a benign reducing agent and sodium cyanide as additive. The presence of cyanide evidenced to have a central role mediating the complex colloidal chemistry that resulted in the bimetallic structure. Mechanistic insights provided by UV-vis analysis, suggested the formation of the bimetallic PdAg nanostructures through a sequential

displacement galvanic reduction process. Supported catalysts were effectively prepared by impregnation of alpha alumina with colloidal suspensions of the metallic NPs. Exhaustive characterization on the colloidal and supported NPs permitted to confirm the bimetallic metal distribution at the nanoscale, in agreement with a fully alloyed PdAg structure.

The series of catalysts were evaluated in the semi-hydrogenation of acetylene in ethylene rich mixtures. The TOP and ethylene selectivity increased with the Ag content, observation consistent with the reported geometric and electronic promotion of Pd by Ag alloying. Out of the tested catalysts, **50Pd50Ag/Al_2O_3** displayed the best catalytic performance (in terms of ethylene selectivity, TOF and deactivation rate) still superior compared to monometallic Pd commercial references. These results evidenced the applicability of catalysts prepared by our novel synthetic approach in a gas-phase reaction of industrial relevance. This synthetic methodology succeeded in combining several strategies that current nanoengineering provide for the preparation of highly structured materials with potential as ultra-selective catalysts: promotion of the Pd active phase with Ag, C-doping, use of HHDMA as beneficial stabilizer, and fine-tuning the nanoparticle size.

Experimental Section

General method for the synthesis of bimetallic PdAg NPs and monometallic Pd NPs

Bimetallic PdAg NPs were synthesized in water by simultaneous reduction of a mixture of $Pd(NO_3)_2$ and $AgNO_3$ with three defined molar ratios (**50Pd50Ag**; **75Pd25Ag**; **90Pd10Ag**) in the presence of NaCN as additive, HHDMA as the stabilizer and using hydrogen gas as the reducing agent. In the three cases, the amount of NaCN used was 2.05 eq. vs. the amount of palladium, and the HHDMA:M ratio was 10.

As a general method, in a Fischer-Porter bottle the required amount of $AgNO_3$ and NaCN are initially dissolved in water. Subsequently, aqueous HHDMA (30 wt% in water) is added over this solution and the mixture heated at 110 ºC during 15 min. Then, a freshly prepared solution of $Pd(NO_3)_2$ was added over the hot mixture and the resulting heated during 8 min more. Next, the Fischer-Porter bottle is pressurized with 5 bar of H_2 under magnetic stirring and the heating maintained at 110 ºC during 2 h. Next, the Fischer-Porter bottle is cooled down, depressurized and the colloidal suspension used for TEM and UV-Vis analysis. Isolation of the NPs required for further characterization was performed by centrifugation of the colloidal suspension employing acetone as precipitating agent followed by drying under vacuum.

Monometallic Pd NPs (**100Pd0Ag**) were prepared using an analogous procedure to the described for the bimetallic NPs but in the absence of silver. The detailed procedure employed for each NPs is described in the Supporting Information (section 1.2).

Immobilization of colloidal nanoparticles onto α-Al_2O_3

The immobilization of NPs on alpha alumina was performed using acetone as precipitating agent. As a general method, a defined amount of α-Al_2O_3 was suspended in water. Next, the corresponding volume of colloidal nanoparticles (to prepare a 0.5 wt% Pd catalyst) is added over the alumina suspension and the mixture stirred magnetically. Several cycles of stirring and sonication are necessary to assure the full homogenization of the suspension. Subsequently, 15 ml of acetone (half of the volume of water contained in the NPs/Al_2O_3 suspension) are added dropwise over the stirred suspension at a rate of 0.6 ml/min. The mixture is stirred for 35 min more and then filtered using a Teflon filter (pore size, 0.45 μm). The obtained grey solid is washed

and filtered repeatedly using a water-acetone mixture (2:1 v/v). The washed catalyst, free of HHDMA and salt residues, is dried overnight under vacuum at 70 ºC.

Catalytic evaluation

A tubular reactor (3.87 mm internal diameter) was loaded in this order with: 1.0340 g SiC (silicon carbide), a mixture of 0.0227 g of **50Pd50Ag/Al_2O_3** catalyst with 0.5802 g of SiC (as diluting agent), and 0.4013 g SiC. The tube is then attached to the reactor, and a flow of 50 ml/min of N_2 is passed through while it is pressurized at 1 bar. A N_2 flow is used while the reactor is heated at the reaction temperature (50 ºC) using an ethyleneglycol/water bath (30/70, v/v). Once the temperature is stabilized, the gas flow is switched from the reactor towards the by-pass, and then the MFCs of N_2, the gas mixture (ethylene, acetylene, ethane and argon), and H_2 are set to 99.657, 32.393 and 6.950 ml/min respectively. After 5 min of stabilization, the gas mixture is analyzed by GC-TCD to confirm the typical relative composition of this mixture (91.02 % C_2H_4, 4.44 % C_2H_6, 4.54 % C_2H_2) and the peak abundances in comparison to previous zeros. Then the reaction is started by switching the gas mixture from the by-pass towards the reactor tube. After 5 min of reaction, the first GC analysis is performed and then repeated every 16-30 min during the entire reaction test. Analysis of the obtained GC data is constantly necessary to monitor the acetylene conversion. According to the operation mode of iso-conversion, it should be maintained at 70% approx. by the modification of the total flow. At early reaction times, frequent flow adjustments are necessary (until the steady state is reached). At the end of the catalytic test, the flow is switched to N_2 (100 ml/min) during 5 min, the reactor is cooled down, and then the tube is demounted from the reactor skeleton. In order to extract any hydrocarbon products contained in the catalyst bed, 10 ml of pentane are added to the top of the reactor using a syringe. The organic phase is collected in a 10 ml volumetric flask and then 5 ul of bicyclohexyl is added as internal standard. Analysis of the extracted catalysis by GC-MS (HP-5 column) determines the potential presence of green oil. In general, only traces of C_{14}-C_{26} hydrocarbons were detected (only hydrocarbons with even number of carbons). Due to the trace amounts of these products, they were not included in the analysis. Conversion of C_2H_2 and selectivity of C_2H_2 to C_2H_4, C_2H_6 and C_{4s} were calculated from the relationships detailed in the Supporting Information (section 4.1).

Acknowledgements

The authors are grateful to Total Research & Technology Feluy, the Ministerio de Economia y Competividad and the Fondo Europeo de Desarrollo Regional FEDER (CTQ2016-75016-R, AEI/FEDER,UE; PID2019-104427RB-I00) and the Generalitat de Catalunya (SGR2017) for financial support. The authors also thank the experimental contributions by Sanchez, O., Maxime P., Molinet C., Letellier C. at early stages of this project.

Keywords: Bimetallic, PdAg nanoparticles, HHDMA, selective hydrogenation, acetylene in ethylene rich mixtures

References

1. S. Carenco, X. F. Le Goff, J. Shi, L. Roiban, O. Ersen, C. Boissière, C. Sanchez and N. Mézailles, *Chem. Mater.*, 2011, **23**, 2270-2277.
2. S. Carenco, A. Leyva-Pérez, P. Concepción, C. Boissière, N. Mézailles, C. Sanchez and A. Corma, *Nano Today*, 2012, **7**, 21-28.
3. X. Shi, Y. Lin, L. Huang, Z. Sun, Y. Yang, X. Zhou, E. Vovk, X. Liu, X. Huang, M. Sun, S. Wei and J. Lu, *ACS Catal.*, 2020, **10**, 3495-3504.
4. J. Hori, K. Murata, T. Sugai, H. Shinohara, R. Noyori, N. Arai, N. Kurono and T. Ohkuma, *Adv. Synth. Catal.*, 2009, **351**, 3143-3149.
5. A. Yarulin, I. Yuranov, F. Cárdenas-Lizana, P. Abdulkin and L. Kiwi-Minsker, *J. Phys. Chem. C*, 2013, **117**, 13424-13434.
6. N. Lopez and C. Vargas-Fuentes, *Chem. Commun.*, 2012, **48**, 1379-1391.
7. A. Jung, A. Jess, T. Schubert and W. Schütz, *Applied Catalysis A: General*, 2009, **362**, 95-105.
8. G. Vilé, N. Almora-Barrios, S. Mitchell, N. López and J. Pérez-Ramírez, *Chem. Eur. J*, 2014, **20**, 5926-5937.
9. L. Montiel, J. A. Delgado, M. Novell, F. J. Andrade, C. Claver, P. Blondeau and C. Godard, *ChemCatChem*, 2016, **8**, 3041-3044.
10. M. Diaz de los Bernardos, S. Perez-Rodriguez, A. Gual, C. Claver and C. Godard, *Chem. Commun.*, 2017, **53**, 7894-7897.
11. J. A. Delgado, O. Benkirane, C. Claver, D. Curulla-Ferre and C. Godard, *Dalton Trans.*, 2017, **46**, 12381-12403.
12. J. A. Delgado and C. Godard, in *Recent Advances in Nanoparticle Catalysis*, eds. P. van Leeuwen and C. Claver, Springer, Cham, Molecular Catalysis, 2020, vol. 1.
13. G. X. Pei, X. Y. Liu, A. Wang, A. F. Lee, M. A. Isaacs, L. Li, X. Pan, X. Yang, X. Wang, Z. Tai, K. Wilson and T. Zhang, *ACS Catal.*, 2015, **5**, 3717-3725.
14. Q. Feng, S. Zhao, Q. Xu, W. Chen, S. Tian, Y. Wang, W. Yan, J. Luo, D. Wang and Y. Li, *Adv. Mater.*, 2019, **31**, 1901024.
15. Y. Wang, Y. Qi, M. Fan, B. Wang, L. Ling and R. Zhang, *Green Energy Environ.*, 2020, DOI: https://doi.org/10.1016/j.gee.2020.10.020.
16. Z. Li, M. Hu, J. Liu, W. Wang, Y. Li, W. Fan, Y. Gong, J. Yao, P. Wang, M. He and Y. Li, *Nano Research*, 2021, DOI: 10.1007/s12274-021-3849-2.
17. F. Liu, Y. Xia, W. Xu, L. Cao, Q. Guan, Q. Gu, B. Yang and J. Lu, *Angew. Chem. Int. Ed.*, 2021, **60**, 19324-19330.
18. A. Roucoux, J. Schulz and H. Patin, *Chem. Rev.*, 2002, **102**, 3757-3778.
19. P. Witte, P. Berben, S. Boland, E. Boymans, D. Vogt, J. Geus and J. Donkervoort, *Top. Catal.*, 2012, **55**, 505-511.
20. P. T. Witte, S. Boland, F. Kirby, R. van Maanen, B. F. Bleeker, D. A. M. de Winter, J. A. Post, J. W. Geus and P. H. Berben, *ChemCatChem*, 2013, **5**, 582-587.
21. T. Mallat and A. Baiker, *App. Catal. A Gen.*, 2000, **200**, 3-22.
22. H. Zhang, Y. Yang, W. Dai, D. Yang, S. Lu and Y. Ji, *Catal. Sci. Technol.*, 2012, **2**, 1319-1323.
23. T. Mitsudome, T. Urayama, K. Yamazaki, Y. Maehara, J. Yamasaki, K. Gohara, Z. Maeno, T. Mizugaki, K. Jitsukawa and K. Kaneda, *ACS Catal.*, 2016, **6**, 666-670.
24. D. A. Lomelí-Rosales, J. A. Delgado, M. Díaz de los Bernardos, S. Pérez-Rodríguez, A. Gual, C. Claver and C. Godard, *Chem. Eur. J*, 2019, **25**, 8321-8331.
25. A. Yarulin, I. Yuranov, F. Cárdenas-Lizana, D. T. L. Alexander and L. Kiwi-Minsker, *App. Catal. A Gen.*, 2014, **478**, 186-193.
26. C. F. Calver, P. Dash and R. W. J. Scott, *ChemCatChem*, 2011, **3**, 695-697.
27. M. Crespo-Quesada, J.-M. Andanson, A. Yarulin, B. Lim, Y. Xia and L. Kiwi-Minsker, *Langmuir*, 2011, **27**, 7909-7916.
28. M. Crespo-Quesada, F. Cárdenas-Lizana, A.-L. Dessimoz and L. Kiwi-Minsker, *ACS Catal.*, 2012, **2**, 1773-1786.

29. T. Ohba, H. Kubo, Y. Ohshima, Y. Makita, N. Nakamura, H. Uehara, S. Takakusagi and K. Asakura, *Bull. Chem. Soc. Jpn.*, 2017, **90**, 720-727.
30. K. Okitsu, Y. Mizukoshi, H. Bandow, T. A. Yamamoto, Y. Nagata and Y. Maeda, *J. Phys. Chem. B*, 1997, **101**, 5470-5472.
31. W. Guobin, D. Wei, L. Qian, C. Weiliang and Z. Jingchang, *China Pet. Process. Pe.*, 2012, **14**, 59-67.
32. Y. Zhang, W. Diao, J. R. Monnier and C. T. Williams, *Catal. Sci. Technol.*, 2015, **5**, 4123-4132.
33. J. Rebelli, A. A. Rodriguez, S. Ma, C. T. Williams and J. R. Monnier, *Catal. Today*, 2011, **160**, 170-178.
34. L. F. Liotta, A. M. Venezia, G. Deganello, A. Longo, A. Martorana, Z. Schay and L. Guczi, *Catal. Today*, 2001, **66**, 271-276.
35. A. M. Venezia, L. F. Liotta, G. Deganello, Z. Schay and L. Guczi, *J. Catal.*, 1999, **182**, 449-455.
36. P. Weightman and P. T. Andrews, *J. Phys. C*, 1980, **13**, 3529.
37. P. Steiner and S. Hüfner, *Solid State Commun.*, 1981, **37**, 79-81.
38. S. Kunz and E. Iglesia, *J. Phys. Chem. C*, 2014, **118**, 7468-7479.
39. A. W. Hull, *Phys. Rev.*, 1921, **17**, 571.
40. G. Becherer, Ifland, R. , *Naturwissenschaften*, 1954, **41**, 471.
41. Y. Zhang, W. Diao, C. T. Williams and J. R. Monnier, *App. Catal. A Gen.*, 2014, **469**, 419-426.
42. A. Pachulski, R. Schödel and P. Claus, *App. Catal. A Gen.*, 2011, **400**, 14-24.
43. R. Van Hardeveld and F. Hartog, *Surf. Sci.*, 1969, **15**, 189-230.
44. M. Li and J. Shen, *Mater. Chem. Phys.*, 2001, **68**, 204-209.
45. P. S. Cremer, X. Su, Y. R. Shen and G. A. Somorjai, *J. Am. Chem. Soc.*, 1996, **118**, 2942-2949.
46. O. Mamun, K. T. Winther, J. R. Boes and T. Bligaard, *Sci. Data*, 2019, **6**, 76.
47. C. W. A. Chan, K. Y. Tam, J. Cookson, P. Bishop and S. C. Tsang, *Catal. Sci. Technol.*, 2011, **1**, 1584-1592.

Table of Contents entry

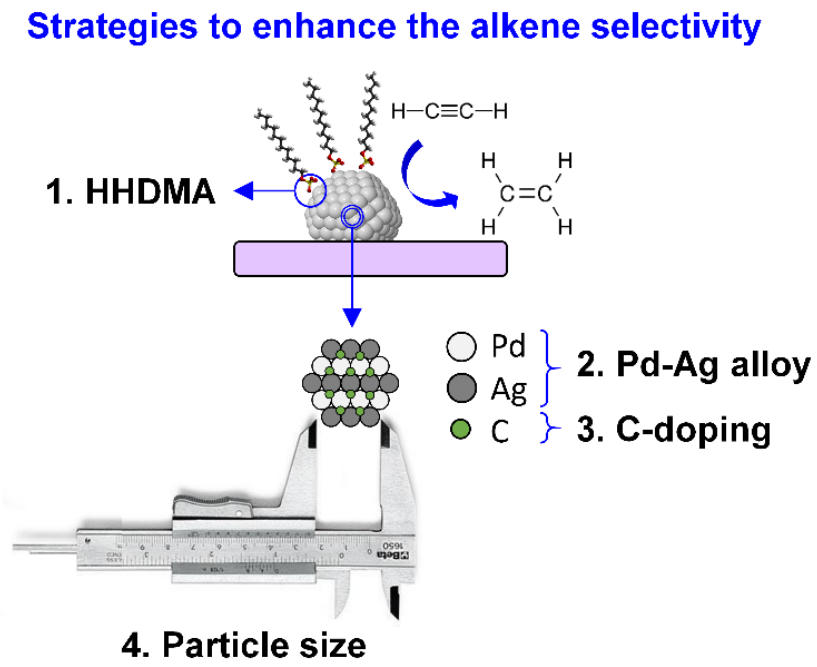

Here we report the synthesis of highly functionalized nanomaterials carefully nanoengineered to catalyze the semi-hydrogenation of acetylene in ethylene rich mixtures. Surface functionalization and structure modification of a series of bimetallic PdAg nanoparticles was performed using HHDMA as stabilizer and alloying the active palladium phase with silver. The reactivity of these materials demonstrated the applicability of HHDMA stabilized NPs in a gas phase reaction of industrial interest and the success of combining several strategies for the enhancement of the alkene selectivity.